Biophysical Chemistry 253 (2019) 106219

Contents lists available at ScienceDirect

Biophysical Chemistry

journal homepage: www.elsevier.com/locate/biophyschem

Aggregation kinetics of short peptides: All-atom and coarse-grained molecular dynamics study

Beata Szała, Andrzej Molski*

Adam Mickiewicz University in Poznań, Faculty of Chemistry, Umultowska 89b, 61-614 Poznań, Poland

HIGHLIGHTS

- MARTINI and OPLS-AA aggregation kinetics are similar for Ala8, Asn8, and GNN.
- In the initial stage of aggregation small clusters grow by monomer addition.
- In the second stage the dominant cluster growth path is cluster-cluster coalescence.
- The sequence-specific differences show up in the second step of aggregation.

GRAPHICAL ABSTRACT

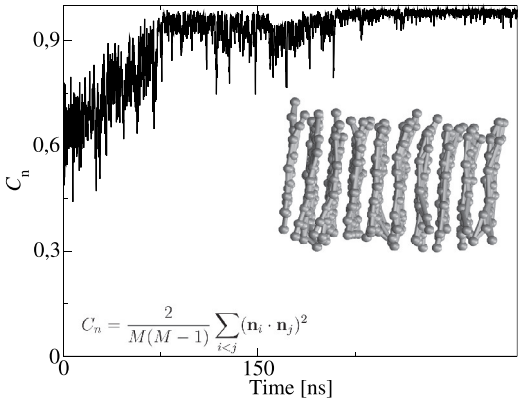

ARTICLE INFO

Keywords:
Peptides
Aggregation kinetics
Molecular dynamics
OPLS-AA
MARTINI

ABSTRACT

Peptides can aggregate into ordered structures with different morphologies. The aggregation mechanism and evolving structures are the subject of intense research. In this paper we have used molecular dynamics to examine the sequence-dependence of aggregation kinetics for three short peptides: octaalanine (Ala8), octaasparagine (Asn8), and the heptapeptide GNNQQNY (abbreviated as GNN). First, we compared the aggregation of 20 randomly distributed peptides using the coarse-grained MARTINI force field and the atomistic OPLS-AA force field. We found that the MARTINI and OPLS-AA aggregation kinetics are similar for Ala8, Asn8, and GNN. Second, we used the MARTINI force field to study the early stages of aggregation kinetics for a larger system with 72 peptides. In the initial stage of aggregation small clusters grow by monomer addition. In the second stage, when the free monomers are depleted, the dominant cluster growth path is cluster-cluster coalescence. We quantified the aggregation kinetics in terms of rate equations. Our study shows that the initial aggregation kinetics are similar for Ala8, Asn8, and GNN but the molecular details can be different, especially for MARTINI Ala8. We hypothesize that peptide aggregation proceed in two steps. In the first step amorphous aggregates are formed, and then, in the second step, they reorganize into ordered structures. We conclude that sequence-specific differences show up in the second step of aggregation.

* Corresponding author.
E-mail addresses: beata.szala@amu.edu.pl (B. Szała), amolski@amu.edu.pl (A. Molski).

https://doi.org/10.1016/j.bpc.2019.106219
Received 8 April 2019; Received in revised form 14 June 2019; Accepted 3 July 2019
Available online 05 July 2019
0301-4622/

1. Introduction

A detailed understanding of aggregation kinetics of peptides is important both for the development of functional biomaterials and for the development of therapies against protein misfolding diseases [1].

Molecular dynamics simulations can explore aggregation kinetics at the molecular level that is difficult to access experimentally. All-atom (AA) molecular dynamics models only probe small systems at early stages of aggregation. Coarse-grained (CG) models allow longer simulations of larger systems so general characteristics of the thermodynamics and kinetics of aggregation can be obtained. Applications of AA and CG models for protein aggregation were recently reviewed in [2–4].

One direction to study the mechanism of protein aggregation is to use peptide fragments as model systems [5]. Short peptides, typically 2–10 residues, have been the subject of many AA and CG simulations. Explicit solvent AA simulations provide the most detailed information on the cluster formation process [4]. In most kinetic studies randomly dispersed monomer are allowed to aggregate freely even though enhanced sampling techniques can also provide kinetic information [6,7]. AA simulations use different force fields, e.g. GROMOS [8], OPLS-AA [9], CHARMM [10], AMBER [11], and different water models, e.g. SPC [12] and TIP3P [13]. Comparative studies of peptide aggregation propensities showed inconsistencies between AA force fields, however, it is not clear which AA force field is currently the best or recommended model [4].

Several CG force fields with sequence specificity have been used to study aggregation of short peptides [2]. MARTINI is a popular CG force field that uses a four to one mapping scheme, i.e. four heavy atoms together with associated hydrogen atoms are represented by a single CG bead [14]. Consistently, MARTINI water beads correspond to four real water molecules. However, MARTINI requires a secondary structure assignment. The peptideB implicit solvent model has a more detailed coarse-grained mapping than MARTINI [15]. As peptideB does not fix the secondary structure it can be used explore cluster structures. PeptideB uses Langevin dynamics for molecular motions. The PRIME implicit solvent model also allows secondary structure changes [16]. It makes use of discontinuous molecular dynamics (DMD) which provides additional speed up.

In this work we use AA and CG molecular dynamics simulations to study aggregation kinetics of three short polypeptides: alanine octapeptide (Ala8), asparagine octapeptide (Asn8) and the heptapeptide GNNQQNY (abbreviated as GNN). Homopetide repeats of alanine and asparagine are prevalent in eukaryotes [17]. Due to its simplicity, polyalanine is a good reference peptide to study the effect of side-chains on aggregation. Molecular dynamics has been employed to study aggregation of alanine and asparagine homopetides [18–24] and GNN [25–37]. Those studies indicated that the aggregation kinetics and evolving morphologies depend on the peptide sequence. Moreover, different force fields lead to one-step or two-step aggregation [38]. In one-step aggregation free peptide monomers aggregate directly into ordered clusters. In the first step of two-step aggregation free monomers aggregate into disordered clusters. In the second step the initial metastable clusters reorganize into ordered structures.

The purpose of this work is to gain further insight into sequence-dependent aggregation kinetics of short peptides Ala8, Asn8, and GNN. First, we compared aggregation kinetics and cluster morphologies generated by the atomistic OPLS-AA force field and the CG MARTINI force field for small systems with 20 peptides. We found that the CG MARTINI force field reproduces the AA aggregation kinetics of Ala8, Asn8 and GNN. This justifies the use of the MARTINI force field to study larger system at longer times. Second we simulated the aggregation kinetics with the CG MARTINI force field for 72 peptides and explored the concentration dependence of aggregation. We found that the aggregation kinetics can be approximately described by rate equations, which suggests that the aggregation mechanism does not change with the initial peptide concentration. Third we used the MARTINI force field to explore the system-size dependence of aggregation kinetics for Ala8. We found that the aggregation mechanism changes with the system size. For small systems we observed aggregation leading directly to a single cluster whereas for larger systems several clusters are formed initially and those clusters coalesce into a single cluster.

The conclusions of our work depend on the quality of the force fields applied. It is well known that even atomistic force fields may not represent aggregation propensities accurately [39–41]. For instance, Carballo-Pacheco et al. [41] showed that OPSA-AA predicts the aggregation of peptides which are known experimentally not to aggregate. Also coarse-grained models may fail to describe aggregation accurately. For instance, Javanainen et al. [42] showed that MARTINI causes excessive aggregation of membrane proteins.

This paper is organized as follows. In the next section we present details of simulations and data analysis. The results of simulations are presented in Section 3. First, we demonstrate consistency between the OPLS-AA and CG MARTINI simulations for Ala8, Asn8, and GNN. Then we focus on the concentration and system-size effects for aggregation using the MARTINI force field. In Section 4 we discuss the origin of differences between aggregation propensities for Ala8, Asn8, and GNN. Finally in Section 5 we present summary and conclusions.

2. Methods

In this work we focus on aggregation kinetics of Ala8, Asn8, GNN and find that the aggregation kinetics for OPLS-AA and MARTINI are similar, although the molecular details are different.

2.1. Simulations

Atomistic OPLS-AA simulations and CG MARTINI simulations were performed using GROMACS 4.6.5 software package [43].

2.1.1. OPLS-AA

The OPLS-AA simulations were performed with the TIP3P water with a time step of 2 fs and periodic boundary conditions applied in all directions. For the van der Waals interactions a cut-off of 1 nm was used. The temperature was maintained at 303 K via the velocity rescaling algorithm with a stochastic term. Pressure was maintained at 1 bar with the Parrinello-Rahman barostat. The OPLS-AA simulations were repeated twice for each peptide.

The OPLS-AA force field was used to simulate aggregation of a small system with $N = 20$ peptides randomly dispersed in a box of size 13.05 nm. The simulation box contained about 73,000 TIP3P water molecules which corresponds to a concentration of 15 mM. The simulated time was 180 ns in each case.

2.1.2. MARTINI

The CG simulations were performed with the MARTINI 2.2 force field [44,45] which is a CG force field for proteins, lipids, and carbohydrates. The MARTINI force field and its modifications have been previously used to study peptide aggregation [46–53]. A detailed description of the MARTINI model is given in [44,54]. Periodic boundary conditions were applied in all directions. Temperature was maintained at 303 K via the Berendsen thermostat. Pressure was maintained at 1 bar via the Berendsen barostat. A cut-off of 1.2 nm was used for the van der Waals interactions.

To assign the secondary structure for MARTINI beads we performed short OPLS-AA simulations of single peptides in water and determined the distribution of secondary structures by using the VMD timeline plugin [55] and the Gromacs do_dssp tool [43]. The most populated structure for all examined peptides was random coil but various types of beta-type structures had significant contributions too: 30% for Ala8, 44% for Asn8, and 13% for GNN. The least populated were the helix-type structures. Our preliminary MARTINI simulations showed that

Table 1
Summary of MARTINI simulations used to explore the concentration effect on Ala8, Asn8, and GNN aggregation. Temperature 303 K.

Concentration [mM]	Number of monomers	Approx. number of water beads	Box size [nm]	Simulated time [ns] Ala8 Asn8 GNN
35	72	29,000	15	600 500 300
15	72	64,000	20	800 800 800
8	72	125,000	25	600 600 500
4	72	227,000	30	1250 1250 1100

Ala8 aggregates for all secondary structures (coild, extended, helix) but Asn8 and GNN with random coil beads do not aggregate whereas Asn8 and GNN with extended and helix beads do aggregate (cf. Fig. S1 in Supplementary Information). This implied that either the extended or helix structure could be assigned to Asn8 and GNN. In order to bring out and rationalize the sequence dependence of aggregation kinetics it is convenient to have the same secondary structure type for all MARTINI beads. Because the aggregation prone helix-type structures were least populated, we decided to apply the extended type to all MARTINI beads used in this work. This was justified a posteriori by the consistency of the MARTINI and OPLS-AA aggregation kinetics.

Three sets of MARTINI simulations were performed to compare Ala8, Asn8, and GNN aggregation kinetics. The first set was designed to compare AA and CG simulations. We studied aggregation kinetics of Ala8, Asn8, and GNN for a small system with $N = 20$ MARTINI peptides randomly dispersed in a box of size 13.05 nm containing about 17,200 water beads. This corresponds to a peptide concentration of 15 mM as in AA simulations. The simulated time was 800 ns and each simulation was repeated twice.

In the second set of MARTINI simulations (cf. Table 1) we increased the system size to $N = 72$ and explored the concentration effect on aggregation kinetics for Ala8, Asn8, and GNN. Peptides were randomly placed in boxes of different sizes at concentrations from 4 mM to 35 mM. Each simulation was repeated three times.

In the third set of MARTINI simulations we explored the finite-size effects on Ala8 aggregation kinetics. The concentration of Ala8 was kept at $c_0 = 15$ mM and the simulated time was 800 ns. The number of Ala8 peptides and the box size varied as shown in Table 2.

2.1.3. Modified MARTINI simulations

The MARTINI model pre-assigns the secondary structure and does not define H-bonds explicitly. In general, this may lead to different aggregation kinetics of OPLS-AA petides and the corresponding MARTINI peptides [47,53]. In our preliminary simulations we found, for instance, that the OPLS-AA aggregation kinetics of glutamine octapeptide Gln8 are not well represented by the MARTINI force field, although MARTINI Gln8 is similar to Asn8.

The fourth set of MARTINI simulations was carried out for Gln8 to explain the different behavior of MARTINI Asn8 and Gln8. Aggregation of Gln8 was simulated with the original and modified MARTINI parameters. In these simulations glutamine was mapped using the original MARTINI backbone bead (Nda) and a side chain bead (P4) with variable BB-SC interactions, $\varepsilon = 4.0$–4.5 kJ/mol. The meaning of the bead symbols Nda and P4 is given in Table S1 in Supplementary Information. The initial monomer number was $N = 72$ and concentration $c_0 = 15$ mM. The simulated time was 600 ns.

Table 2
Summary of MARTINI simulations used to explore the system-size effect on Ala8 aggregation. Temperature 303 K. Concentration about $c_0 = 15$ mM. Simulated time 800 ns.

Number of Ala8-monomers	Approx. number of water beads	Box size [nm]	Replicas
3	2530	7.00	10
6	5220	8.75	10
9	7760	10.00	10
15	13,820	11.85	10
20	17,230	13.05	10
30	29,870	15.00	10
72	64,000	20.00	3

2.2. Data analysis

2.2.1. Cluster analysis

We refer to a peptide molecule as a monomer. We refer to an aggregate made up of two or more peptides as a cluster. A peptide belongs to a cluster when the center of any of its atoms is less than a cut-off distance of 0.5 nm from the center of an atom of another peptide in that cluster.

To analyze aggregation we used several descriptors: N_m – the number of free monomers; N_c – the number of clusters (dimers, trimers and higher order aggregates); M – the size of a cluster, i.e. the number of peptides in the cluster; R_g – the radius of gyration of a cluster; b – the asphericity of a cluster, defined as $b = \lambda_z^2 - (\lambda_x^2 + \lambda_y^2)/2$ where λ_x, λ_y, λ_z are the principal moments of the gyration tensor and the axes are chosen such that $\lambda_x^2 \le \lambda_y^2 \le \lambda_z^2$; and C_n- the end-to-end correlation parameter of a cluster defined as [56].

$$C_n = \frac{2}{M(M-1)} \sum_{i<j} (\mathbf{n}_i \cdot \mathbf{n}_j)^2 \tag{1}$$

where the unit vector $\mathbf{n}_i$ is oriented from the first to the last backbone atom of peptide i. The correlation parameter C_n is normalized in such a way that for uncorrelated $\mathbf{n}_i$ vectors the parameter assumes the value 1/3 whereas for correlated $\mathbf{n}_i$-s it tends to 1.

To characterize peptide-peptide encounters we used the collision acceptance probability (CAP) defined as $(n_{\text{bind}} - n_{\text{unbind}})/n_{\text{bind}}$, where n_{bind} is the number of monomer binding events and n_{unbind} is the number of events where a monomer unbinds from a cluster [41].

Due to periodic boundary conditions, a cluster that crosses a boundary gets split and is represented in the simulation box as two or more split clusters. To properly calculate cluster descriptors, these split clusters are merged into a single clusters before a descriptor is calculated.

2.2.2. Rate equations

In our simulations peptide aggregation is dominated by three types of molecular events: aggregation of two monomers into a dimer (smallest cluster), addition of a monomers to clusters, and cluster-cluster coalescence. In an attempt to quantify aggregation kinetics we focused on the following kinetic model

$$\frac{dc_m}{dt} = -2k_1 c_m^2 - k_2 c_m c_c \tag{2}$$

$$\frac{dc_c}{dt} = +k_1 c_m^2 - k_3 c_c^2 \tag{3}$$

where c_m is the number concentration of free monomers and c_c is the number concentration of all clusters, $c_c = \Sigma_i c_{c,\,i}$, where $c_{c,\,i}$ is the number concentration of clusters of size $i \ge 2$. According to Eq. (2), free monomers decay by formation of dimers with rate constant k_1 and by attachment to the existing clusters with rate constant k_2. According to Eq. (3), clusters are generated by fusion of two monomers with rate constant k_1 and decay by binary coalescence with rate constant k_3. Note that Eq. (3) has no term of form $c_m c_c$ as the addition of monomers to clusters does not change the overall number of clusters, although it increases the overall cluster mass. Eqs. (2) and (3) were fitted globally to kinetic data for different initial monomer concentrations c_0 and the rate constants k_1, k_2, and k_3 were estimated by the least-squares fitting.

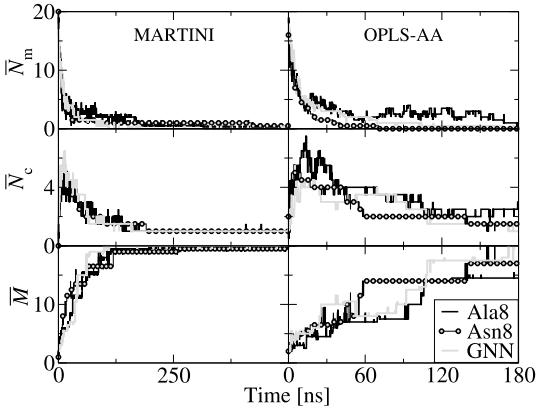

Fig. 1. Average number of free monomers $\overline{N}_m$ (top panels), the average number of clusters $\overline{N}_c$ (mid panels), and average size of the largest cluster $\overline{M}$ (bottom panels) as a function of time for Ala8, Asn8, and GNN: MARTINI (left panels) vs OPLS-AA (right panels) simulations at $N = 20$ and $c_0 = 15$ mM. Note the different time scales.

3. Results

3.1. OPLS-AA vs MARTINI aggregation

3.1.1. Aggregation kinetics

In order to compare AA and CG kinetics we performed OPLS-AA and MARTINI simulations for $N = 20$ randomly dispersed peptides at the initial concentration $c_0 = 15$ mM. Fig. 1 shows the average number of free monomers $\overline{N}_m$ (top panels), the average number of clusters $\overline{N}_c$ (mid panels), and the average size of the largest cluster $\overline{M}$ (bottom panels) as a function of time for Ala8, Asn8, and GNN. The MARTINI (left panels) and OPLS-AA (right panels) kinetics are quite similar. The number of free monomers drops from the initial value to a low value corresponding the saturation concentration. The number of clusters reaches a maximum and than drops to one or two clusters. The size of the largest cluster grows monotonously and reaches a values close to a maximum (20). At the end of simulation one gets one or few clusters depending on the trajectory repeat.

Interestingly, the aggregation half-times $t_{1/2}$ of the average kinetics for AA and CG simulations are comparable: Ala8: $t_{1/2} = 3.6$ ns (AA) and 3.8 ns (CG), Asn8: $t_{1/2} = 2.5$ ns (AA) and 6.6 ns (CG), GNN: $t_{1/2} = 4.5$ ns (AA) and 4.0 ns (CG). For comparison, the aggregation times $t_{3/4}$ to reach one quarter of the initial number of free monomers are: Ala8: $t_{3/4} = 13.9$ ns (AA) and 9.8 ns (CG), Asn8: $t_{3/4} = 10.7$ ns (AA) and 15.3 ns (CG), GNN: $t_{3/4} = 13.4$ ns (AA) and 16.5 ns (CG). The reported times refer to the actual simulation times for the AA and CG simulations, which entails that we do not observe a large speed up factor due to the smoothness of the CG potential [57].

The times t_{max} when the average number of clusters reaches a maximum for the AA and CG simulations are also comparable: Ala8: $t_{max} = 13.8$ ns (AA) and 12.1 ns (CG), Asn8: $t_{max} = 8.2$ ns (AA) and 9.9 ns (CG), GNN: $t_{max} = 12.9$ ns (AA) and 13.5 ns (CG).

Another way to characterize the OPLS-AA and MARTINI aggregation kinetics is to compare the collision acceptance probabilities (CAP) [41]. As seen in Table 3, CAPs are similar except for MARTINI Ala8, where it is much smaller, CAP(Ala8, MARTINI) = 0.06. Note, however, that n_{bind} and n_{unbind} for MARTINI Ala8 are much higher than those for Asn8 and GNN.

3.1.2. Cluster shapes and structures

Fig. 2 shows the radius of gyration R_g of the Ala8 largest cluster as a function of time (solid lines) for MARTINI (top panel) and OPLS-AA (bottom panel) simulations for $N = 20$ and $c_0 = 15$ mM. The R_g time series are scaled by their maximum values along the trajectories.

Table 3
Comparison of the average collision acceptance probability (CAP) for the OPLS-AA an MARTINI force fields for $N = 20$ estimated from the initial 180 ns trajectory segments.

Peptide	OPLS-AA			MARTINI		
	n_{bind}	n_{unbind}	CAP	n_{bind}	n_{unbind}	CAP
Ala8	173	155	0.13	449	430	0.06
Asn8	52	36	0.31	83	64	0.23
GNN	76	60	0.22	80.5	62.5	0.26

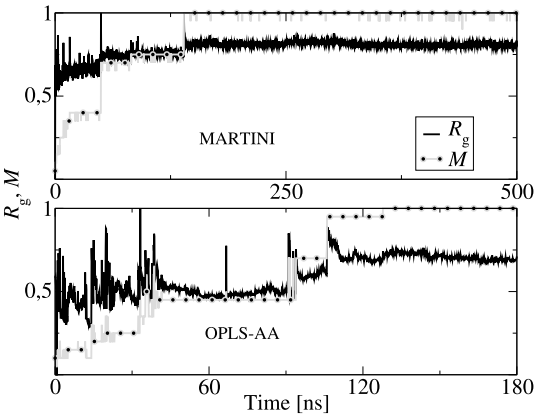

Fig. 2. Aggregation of Ala8 for $N = 20$ and $c_0 = 15$ mM. Top panel: time evolution of the radius of gyration R_g of the largest cluster scaled by its maximum value (solid line) and the size of the largest cluster M scaled by its maximum value (dotted line) for MARTINI simulations. Bottom panel: Same for OPLS-AA simulations. Note the different time scales.

In the course of aggregation, R_g increases to reach a steady value. The noise on the R_g time series has two origins. The low amplitude noise is related to the internal structure fluctuations when the cluster size stays constant. The jumps are related to cluster-cluster coalescence. This is clearly seen by comparing R_g with the size M of the largest cluster (dotted lines). Note that the M time series were also scaled by their maximum values. We found a similar behavior for Asn8 and GNN (cf. Fig. S2 in Supplementary Information).

Fig. 3 shows the asphericity (b – solid line) of the largest GNN cluster from CG (top panel) and AA (bottom panel) simulations at $N = 20$ and $c_0 = 15$ mM. For reference the size of the largest clusters M scaled by its maximum value is added (dotted line). The asphericity

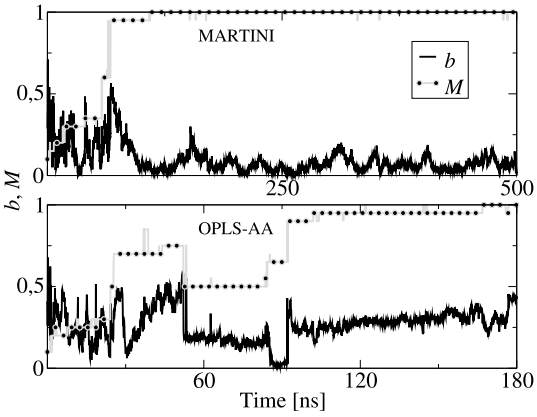

Fig. 3. Asphericity (b – solid line) of the GNN largest cluster and the size of the largest cluster M scaled by its maximum value (dotted line) from MARTINI (top panel) and OPLS-AA (bottom panel) simulations for $N = 20$ and $c_0 = 15$ mM. Note the different time scales.

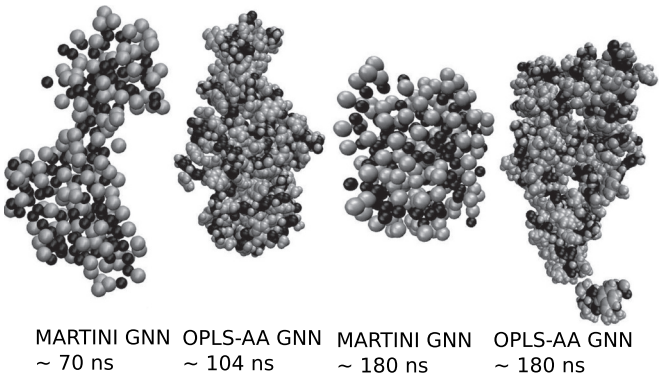

Fig. 4. Snapshots from GNN MARTINI and OPLS-AA simulations at $c_0 = 15$ mM and $N_0 = 20$. The two snapshots on the left are taken when the largest clusters are formed. The two snapshots on the right are taken at 180 ns. The clusters formed by coalescence of two clusters (clusters on the left) have initially extended shapes that evolve into spherical shapes (clusters on the right). The rearrangement is faster for the MARTINI force field.

decreases for the CG MARTINI force field, showing large fluctuations, whereas for the AA OPLS-AA force field the asphericity decreases initially but reaches a steady value when the largest size is reached. We found a similar behavior for Ala8 and Asn8 (cf. Fig. S3 in Supplementary Information). This is consistent with visual inspection of the largest AA and CG clusters (cf. Fig. 4). The clusters formed by coalescence of two clusters (clusters on the left in Fig. 4) have initially extended shapes that show a tendency to evolve into spherical shapes (clusters on the right). The rearrangement is faster for the MARTINI force field. Note that the OPLS-AA largest cluster begins to split at 180 ns. We found a similar behavior for Ala8 and Asn8 (cf. Fig. S4 and S5 in Supplementary Information).

In this work we have used the end-to-end correlation parameter C_n to explore the internal structures of AA and CG aggregates. We found that OPLS-AA and MARINI clusters have disordered structures, $C_n \approx 0.3$, except for the MARTINI Ala8 clusters which are ordered, $C_n \approx 1$..

Fig. 5 shows the C_n time series for coarse-grained simulations of the MARTINI force field (top panels) and the OPLS-AA force field (botom pannels) for Ala8 (left panels) and GNN (right panels). The solid-lines show C_n of the largest cluster. For comparison the dotted lines represent the size M of the largest cluster normalized to its maximum value. For completeness, the C_n time series for Asn8 is presented in Fig. S6 in

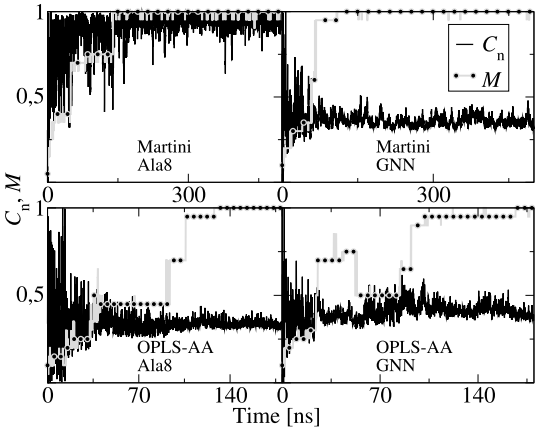

Fig. 5. End-to-end correlation parameter C_n for MARTINI (top panels) and OPLS-AA (bottom panels) simulations of Ala8 (left panels) and GNN (right panels) for $N = 20$ and $c_0 = 15$ mM. Solid-lines: C_n of the largest cluster. Dotted lines: the size M of the largest cluster normalized to its maximum value. Note the different time scales.

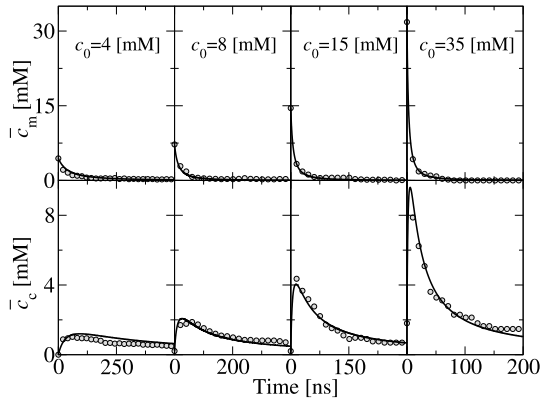

Fig. 6. Time evolution of the average concentration of monomers $\bar{c}_m$ and the average concentration of clusters $\bar{c}_c$ for MARTINI GNN at various initial monomer concentrations c_0 (circles) together with the global fit to rate Eqs. (2) and (3) (solid lines).

Supplementary information. Only MARTINI Ala8 clusters show parallel alignment of peptides (cf. Fig. S3 in Supplementary Information). When two clusters aggregate they may not be aligned properly, which is seen as a drop of C_n. However, such aggregate rearranges quickly into an ordered structure.

3.2. MARTINI aggregation kinetics

In order to explore peptide aggregation kinetics for larger and longer times we performed Martini simulations with $N = 72$ peptides at various initial monomer concentrations c_0.

Fig. 6 shows the time evolution of the average concentration of monomers $\bar{c}_m$ and the average concentration of clusters $\bar{c}_c$ for MARTINI GNN at various initial monomer concentrations c_0 (circles) together with the global fit to rate Eqs. (2) and (3) (solid lines). Similar fits were performed for Ala8 and Asn8 (cf. Fig. S7 and S8 in Supplementary Information). The fitted rate constants are listed in Table 4.

The fits for GNN and Asn8 were quite good but the fit for Ala8 was poorer at low concentrations. This may have two origins. The first is the statistical noise of the simulated kinetics curves for c_m and c_c. The second is an approximate character of rate Eqs. (2) and (3). The global fits to the time trajectories of c_m and c_c suggest that there is no significant change of the kinetic mechanism in the studied concentration range.

We found that both the monomer and cluster kinetics scale with the initial concentration c_0. Fig. 7 illustrates the concentration dependence of the aggregation kinetics for the MARTINI simulations. The aggregation half time $t_{1/2}$ was determined for the average monomer $\overline{N}_m$ decay. The top panel in Fig. 7 shows the scaling of the monomer kinetics: there is a linear correlation between the logarithm of the aggregation half-time, $t_{1/2}$ and the logarithm of the initial monomer concentration c_0. The slope $\gamma_{1/2}$ is -1.61 for Ala8, -0.98 for Asn8, and -1.14 for GNN.

The bottom panel in Fig. 7 shows the scaling for the average cluster kinetics: the logarithm of the time t_{max} when the average number of

Table 4
The global fits of rate Eqs. (2) and (3) to the averaged simulated $\bar{c}_m$ and $\bar{c}_c$ time series together with the estimated standard deviations (in parenthesis).

Rate constant	Ala8	Asn8	GNN
[$mM^{-1}ns^{-1}$]			
k_1	0.0059 (0.0004)	0.0048 (0.0009)	0.0056 (0.0005)
k_2	0.0051 (0.0006)	0.0088 (0.0040)	0.0066 (0.0016)
k_3	0.0116 (0.0012)	0.0032 (0.0011)	0.0046 (0.0004)

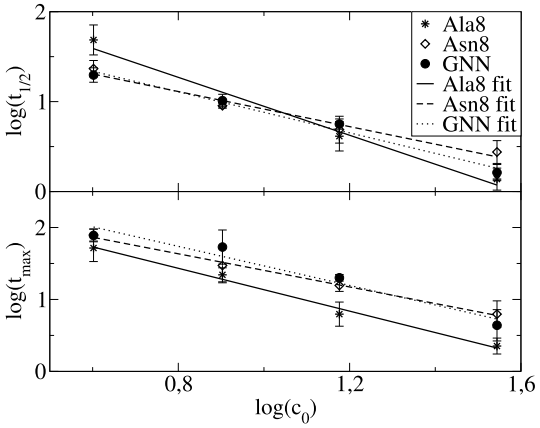

Fig. 7. Concentration dependence of the average aggregation kinetics for coarse-grained simulation for Ala8, Asn8 and GNN at $N = 72$. Top pannel: Logarithm of the aggregation half-time, $t_{1/2}$ vs the logarithm of the initial monomer concentration, c_0. Bottom panel: Logarithm of the time t_{max} when the number of clusters reaches a maximum vs the logarithm of the initial monomer concentration c_0. The error bars indicate the sample standard deviation.

clusters reaches a maximum vs the logarithm of the initial monomer concentration c_0. The slope γ_{max} of the linear correlation between $\log t_{max}$ and $\log c_0$ is -1.49 for Ala8, -1.15 for Asn8, and -1.36 for GNN.

3.3. Finite-size effects

In order to explore the dependence of aggregation on the system size, simulations of MARTINI Ala8 were performed for different numbers of peptides at a constant initial concentration $c_0 = 15$ mM. Fig. 8 shows the average number of free monomers ($\overline{N}_m$ – top panel) and the average largest cluster size ($\overline{M}$ – bottom panel) scaled by the initial number of monomers N. The scaled $\overline{N}_m$ is similar for all system sizes. However, the scaled $\overline{M}$ time series show that the largest cluster growth is slower for larger systems. For larger systems ($N = 30$ and 72) the dominant mechanism of growth at longer times is cluster-cluster coalescence seen us jumps on the $\overline{M}$ time series.

3.4. Modified MARTINI simulations

Fig. 9 shows the number of free Gln8 monomers N_m as a function of time for coarse-grained (top panel) vs all-atom (bottom panel). In AA

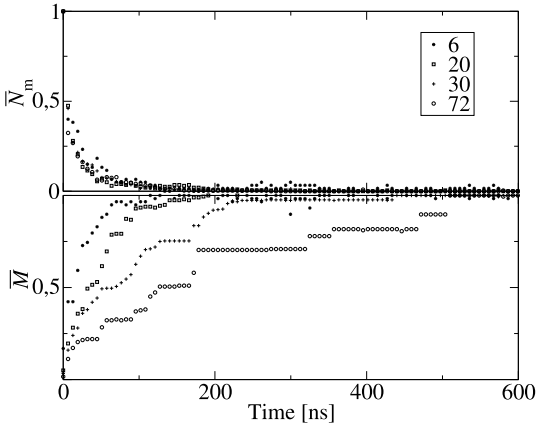

Fig. 8. Finite-size effects for coarse-grained simulations of Ala8 at 15 mM. The average number of free monomers $\overline{N}_m$ (top panel) and the average largest cluster size $\overline{M}$ (bottom panel) scaled by the initial number of monomers N as indicated in the inset.

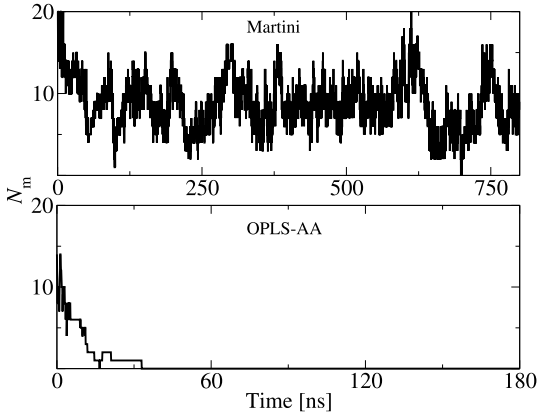

Fig. 9. The number of free monomers N_m as a function of time for Gln8: MARTINI (top panel) vs OPLS-AA (bottom panel) simulations for $N = 20$ and $c_0 = 15$ mM. Note the different time scales.

simulations N_m drops to almost zero, whereas in CG simulations N_m decreases to about one-half of the initial value. Moreover, a single cluster is formed in AA simulations whereas CG simulations produced several cluster undergoing fusion and fission.

Fig. 10 shows the number of free monomers N_m as a function of time for modified MARTINI Gln8 with different interaction strengths between BB-SC beads. The aggregation propensity increases for larger ϵ. This points to the crucial effect of the BB-SC interactions in aggregation of MARTINI polyglutamine.

4. Discussion

4.1. OPLS-AA vs MARTINI aggregation

The aggregation propensity of MARTINI peptides correlate with the interaction strength between MARTINI backbone (BB), side-chain (SC) and water (W) beads [54]. MARTINI Ala8 is a homopeptide with BB (Nda) beads (cf. Tables S1 and S2 in Supplementary Information). MARTINI Ala8 shows the highest propensity for aggregation despite the low interaction strength between two BB chains. Moreover MARTINI Ala8 forms ordered clusters, but Ala8 and GNN form only amorphous clusters. The ordered structure of Ala8 clusters is caused by the lack of side chains in the MARTINI alanine. Alanine backbone beads have a 'hydrophobic' character. The interactions between water and alanine beads and between two alanine beads belonging to different molecules have the same strength ($\epsilon \approx 3.5$ kJ/mol) and are weaker than water-water interaction ($\epsilon \approx 5$ kJ/mol). With this in mind, we suggest that

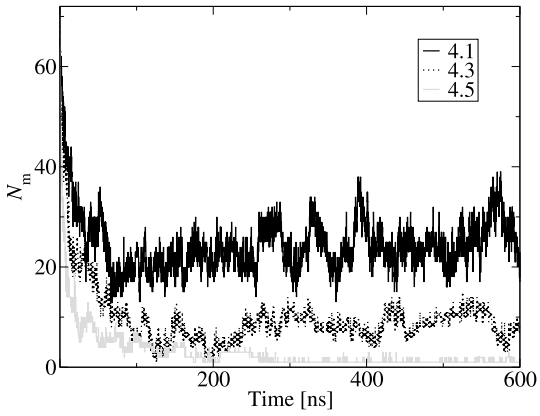

Fig. 10. MARTINI simulations of Gln8 at $N = 72$ and $c_0 = 15$ mM. The number of free monomers N_m as a function of time for different interaction strengths ϵ [kJ/mol] as indicated.

alanine aggregation is caused by the tendency to reduce the number of water-alanine contacts, which results is the aggregate shape with limited solvent-peptide surface.

MARTINI Asn8 is a homopeptide with BB(Nda), SC(P5) beads. The side chain-side chain (SC-SC) and side chain-water interactions (SC-W) are the same ($\epsilon \approx 5.6$ kJ/mol), but the interactions between side chains and backbone (SC-BB, $\epsilon \approx 5.0$ kJ/mol) are stronger than between the backbone and water (BB-W, $\epsilon \approx 4.0$ kJ/mol). The strong SC-BB interactions induce aggregation.

MARTINI GNN is a heteropetide with Nda, P5, P4, SC4 and SP1 beads. To understand GNN aggregation propensity one can represent the GNN-GNN and GNN-water interactions as an average over the GNN sequence. The average was calculated as the sum of individual interactions strengths between all (146) pairs of beads on two chains divided by the number of pairs. The average GNN-GNN and GNN-water interactions are the same $\epsilon \approx 4.3$ kJ/mol. We suggest that there are two reasons why GNN aggregation occurs. First, a slight 'hydrophobic' effect caused by water-water interactions ($\epsilon \approx 5.0$ kJ/mol) that are stronger then average GNN-water interactions. The second reason is the amino-acids sequence. Chains assume such positions in a cluster that reduce the number of unfavorable interactions and thus decrease the potential energy.

4.2. MARTINI aggregation kinetics

The MARTINI model and its modification has been often used to study aggregation of peptides [46,47,49–51,53]. It was found that the aggregation kinetics and the aggregate morphology depend strongly on the peptide sequence.

Interestingly, we found no such strong dependence in our OPLS-AA and MARTINI simulations. The initial aggregation kinetics are similar for OPLS-AA and MARTINI Ala8, Asn8, GNN. The ordered MARTINI Ala8 aggregates are different from the amorphous Asn8 and GNN aggregates. Note, however, that in our OPLS-AA simulations Ala8, Asn8, and GNN form similar disordered aggregates. A different behavior of MARTINI Ala8 may be caused by the lack of side-chain beads.

Also the CAP shows a different behavior of MARTINI Ala8. In ref. [41], a low value of CAP correlates with a lower propensity for aggregation. This is not the case for MARTINI Ala8. The low collision efficiency is compensated by a high number of collision events (cf. Table 3). Visual inspection of trajectories suggests that high values of n_{bind} and n_{unbind} may be related to internal re-organization motions of MARTINI Ala8 clusters. This is consistent with the ordered structure of MARTINI Ala8 aggregates.

In our simulations GNN forms disorderd clusters. The question arises whether longer simulation of MARTINI GNN lead to ordered. We have extended MARTINI GNN simulations to 2.6 μs and not found any ordered or fibril-like structures.

We found in our MARTINI simulations that the characteristic times $t_{1/2}$ and $t_{\max}$ change regularly with the initial concentration c_0. This prompted us to search for a kinetic model of aggregation [58]. The proposed model (2) and (3) describes well the kinetics of c_{m} and c_{c} for different initial concentrations c_0, which suggest the same mechanism for all concentrations studied. However, our kinetic model does not fit the Ala8 data as well as the Asn8 and GNN data, but this may be an artifact due to the simplifications of the MARTINI force field.

4.3. Finite-size effects

The finite-size effects on peptide aggregation kinetics have been noted by several authors [36,59,60]. The focus of those studies was mainly on equilibrium properties. Here we explored the finite-size effect for the kinetics of MARTINI Ala8 and found that the monomer kinetics are similar for different system-sizes but the cluster kinetics are different (cf. Fig. 8). For small systems ($N = 6$ and 20) the time series of the largest cluster size M shows growth by monomer addition. For larger systems, the dominant path is the cluster-cluster coalescence. We hypothesize that the turnover system size is about 30 peptides.

4.4. Modified MARTINI simulations

Glutamine repeats are known from experiment to aggregate effectively [23]. This is consistent with our OPLS-AA simulations but not with our MARTINI simulations (cf. Fig. 9). Molecular structures of Asn8 and Gln8 are similar, however, they behave differently in MARTINI simulations. The difference between OPLS-AA and CG MARTINI simulation for Gln8 correlate with the parameters of MARTINI Gln8 beads. MARTINI Gln8 is a homopeptide with BB(Nda), SC(P4) beads. The side chain-side chain (SC-SC) and side chain-water interactions (SC-W) are the same ($\epsilon \approx 5.0$ kJ/mol). Moreover, the side chain-backbone interactions for different molecules are the same as the water-backbone interactions ($\epsilon \approx 4.0$ kJ/mol). Only the BB-BB interactions contribute to aggregation propensity, because backbone beads interact more strongly with each other ($\epsilon \approx 4.5$ kJ/mol) than with water (or with side chains). Therefore, aggregation of MARTINI polyglutamine is only slightly energetically preferred: aggregates are slightly more stable than monomers surrounded by water. In the case of asparigine, the side chain-side chain and side chain-water interactions are also the same, but the interactions between side chains and backbone are stronger than between water and backbone and, therefore, induce aggregation.

For MARTINI Gln8 aggregation the SC-BB interactions provide the most important contribution to aggregation propensity. To prove this conjecture, we performed a set of simulations with modified SC-BB interaction parameters. An increase of the MARTINI SC-BB attraction leads to enhanced aggregation propensity, modified MARTINI simulations approach all-atom kinetics (cf. Fig. 10). Our modified MARTINI simulations suggest that the MARTINI parameters need to be modified in specific situations, e.g. to reproduce aggregation accurately.

5. Summary and conclusions

In this paper we have examined aggregation kinetics of three short peptides: Ala8, Asn8, and GNN. Those peptides have different structures: Ala8 and Asn8 are homopetides with different side-chains and GNN is a heteropeptide. We have been interested in how the different structures affect early stages of aggregation. To overcome the system-size and simulation-time limitations of molecular dynamics we have focused on the CG MARTINI force field.

First, we validated the MARTINI force field by comparing CG simulations with the OPLS-AA aggregation kinetics for small systems with $N = 20$ peptides. The aggregation kinetics generated by the OPLS-AA and MARTINI force fields are consistent for Ala8, Asn8, and GNN (cf. Fig. 1). The OPLS-AA clusters are disordered and so are the MARTINI Asn8 and GNN clusters. However, MARTINI Ala8 forms ordered clusters (cf. Fig. 5), which we explain by the lack of side-beads for MARTINI Ala8. For the MARTINI force field we rationalized qualitatively the aggregation propensities and cluster morphologies of Ala8, Asn8, GNN by an analysis of the backbone-backbone and backbone-sidechain interactions.

We concluded that the MARTINI force field reproduces essential aspects of the AA aggregation kinetics for Ala8, Asn8, and GNN. However, this may not hold for other sequences, as demonstrated by the Gln8 aggregation kinetics (cf. Fig. 9).

Second, we used the MARTINI force field to study early stages of aggregation kinetics for a larger system with $N = 72$ peptides. In the initial stage small clusters are created that grow by monomer addition. Those small cluster coalesce to form larger clusters. In the second stage, when the free monomers are depleted, the dominant cluster growth path is cluster-cluster coalescence. Accordingly, we have proposed rate Eqs. (2) and (3) that describe the time evolution of the monomer concentration c_{m} and the overall cluster concentration c_{c}. Rate Eqs. (2) and (3) globally fit quite well the simulations for different initial

concentrations (cf. Fig. 6).

Third, the peptide aggregation kinetics are system-size dependent, which can be seen for instance on the largest cluster time coarse (cf. Fig. 8). For small systems ($N = 6$ and 20) we can see the simultaneous cluster creation and growth by monomer addition but we do not see a second stage where, for larger systems, the dominant path would be cluster-cluster coalescence. We found that the time evolution of the largest cluster size is strongly system-size dependent. This raises the question to what extent aggregation pathways in small system (say fewer than 30 peptides) are informative about aggregation in larger systems.

This study shows that the initial aggregation kinetics are similar for Ala8, Asn8, and GNN although the molecular details can be different, especially for MARTINI Ala8. With the exception of MARTINI Ala8, amorphous aggregations are formed. We hypothesize that peptide aggregation proceeds in two steps. In the first step (explored in this work) disordered clusters are formed which, in the second step (not studied here), reorganize to form ordered structures. We conclude that the sequence-specific differences show up in the second step.

The two-step mechanism may be connected with a high concentration of monomers (mM range) used in this work. For example, when two peptides come together they have little time to reorganize before a third one comes along. However, aggregation experiments are carried out in the μM range where intermolecular distances are larger and cluster may have time to rearrange. If so a one-step mechanism emerges.

It is also fair to note that the conclusions of our work depend on the force fields applied. Both OPLS-AA and MARTINI may fail to describe aggregation accurately [39–42]. Although, OPLS-AA and MARTINI predict different molecular details for Ala8, Asn8 and GNN aggregation, both force fields predict consistent aggregation kinetics for systems of size $N = 20$. This leads us to believe that our simulations capture the essential features of Ala8, Asn8, and GNN aggregation.

Acknowledgments

This work was supported by intramural funds of Faculty of Chemistry of Adam Mickiewicz University and by grant no. POWR.03.02.00-00-l026/16 co-financed by the EU through the European Social Fund under the Operational Program Knowledge Education Development.

Appendix A. Supplementary data

Supplementary data to this article can be found online at https://doi.org/10.1016/j.bpc.2019.106219.

References

[1] C.J. Wilson, A.S. Bommarius, J.A. Champion, Y.O. Chernoff, D.G. Lynn, A.K. Paravastu, C. Liang, M.-C. Hsieh, J.M. Heemstra, Biomolecular assemblies: moving from observation to predictive design, Chem. Rev. 118 (2018) 11519–11574.
[2] C. Wu, J.E. Shea, Coarse-grained models for protein aggregation, Curr. Opin. Struct. Biol. 21 (2011) 209–220.
[3] A. Morriss-Andrews, J.E. Shea, Computational studies of protein aggregation: methods and applications, Annu. Rev. Phys. Chem. 66 (2015) 643–666.
[4] M. Carballo-Pacheco, B. Strodel, Advances in the simulation of protein aggregation at the atomistic scale, J. Phys. Chem. B 120 (2016) 2991–2999.
[5] E. Gazit, Self assembly of short aromatic peptides into amyloid fibrils and related nanostructures, Prion 1 (2007) 32–35.
[6] P. Tiwary, M. Parrinello, From metadynamics to dynamics, Phys. Rev. Lett. 111 (230602) (2013).
[7] L.S. Stelzl, G. Hummer, Kinetics from replica exchange molecular dynamics simulations, J. Chem. Theory Simul. 13 (2017) 3927–3935.
[8] M.M. Reif, P.H. Hünenberger, C. Oostenbrink, New interaction parameters for charged amino acid side chains in the GROMOS force field, J. Chem. Theory Comput. 8 (2012) 3705–3723.
[9] W.L. Jorgensen, J. Tirado-Rives, Potential energy functions for atomic-level simulations of water and organic and biomolecular systems, Proc. Natl. Acad. Sci. U. S. A. 102 (2005) 6665–6670.
[10] A.D.Jr. MacKerell, et al., All-atom empirical potential for molecular modeling and dynamics studies of proteins, J. Phys. Chem. B 102 (1998) 3586–3616.
[11] R. Salomon-Ferrer, D.A. Case, R.C. Walker, An overview of the Amber biomolecular simulation package, Wiley Interdiscip. Rev.: Comput. Mol. Sci. 3 (2013) 198–210.
[12] H.J.C. Berendsen, J.P.M. Postma, W.F. van Gunsteren, J. Hermans, Interaction models for water in relation to protein hydration, in: R. Pullman (Ed.), Intermolecular Forces, Reidel, Netherlands, Dordrecht, 1981, pp. 331–342.
[13] W.L. Jorgensen, J. Chandrasekhar, J.D. Madura, R.W. Impey, M.L. Klein, Comparison of simple potential functions for simulating liquid water, J. Chem. Phys. 79 (1983) 926–935.
[14] S.J. Marrink, D.P. Tieleman, Perspective on the MARTINI model, Chem. Soc. Rev. 42 (2013) 6801–6822.
[15] T. Bereau, M.J. Deserno, Generic coarse-grained model for protein folding and aggregation, J. Chem. Phys. 130 (2009) 235106.
[16] M. Cheon, I. Chang, C.K. Hall, Extending the PRIME model for protein aggregation to all twenty amino acids, Proteins 78 (2010) 2950–2960.
[17] N.G. Faux, S.P. Bottomley, A.M. Lesk, J.A. Irving, J.R. Morrison, M.C. de la Banda, J.C. Whisstock, Functional insights from the distribution and role of homopeptide repeats containing proteins, Genome Res. 15 (2005) 537–551.
[18] H.D. Nguyen, C.K. Hall, Phase diagrams describing fibrillization by polyalanine peptides, Biophys. J. 87 (2004) 4122–4134.
[19] H.D. Nguyen, C.K. Hall, Molecular dynamics simulations of spontaneous fibril formation by random-coil peptides, Proc. Natl. Acad. Sci. U. S. A. 101 (2004) 16180–16185.
[20] H.D. Nguyen, C.K. Hall, Spontaneius fibril formation by polyalanines; discontinous molecular dynamics simulations, J. Am. Chem. Soc. 128 (2006) 1890–1901.
[21] S.P. Carmichael, M.S. Shell, A new multiscale algorithm and its application to coarse-grained peptide models for self-assembly, J. Phys. Chem. B 116 (2012) 8383–8393.
[22] Y. Mu, B. Tang, M. Yu, Length-dependent β-sheet growth mechanisms of polyalanine peptides in water and on hydrophobic surfaces, Phys. Rev. E 89 (032711) (2014).
[23] X. Lu, R. Murphy, Asparagine repeat peptides: aggregation kinetics and comparison with glutamine repeats, ACS Chem. Neurosci. 54 (2015) 4784–4794.
[24] Y. Zhang, V.H. Msan, C. Roland, C. Sagui, Amyloid properties of asparagine and glutamine in prion-like proteins, ACS Chem. Neurosci. 7 (2016) 576–587.
[25] J. Gsponer, U. Habertuer, A. Caflish, The role of side-chain interactions in the early steps of aggregation: molecular dynamics simulations of an amyloid-forming peptide from the yeast prion Sup35, Proc. Natl. Acad. Sci. U. S. A. 100 (2003) 5154–5159.
[26] B. Strodel, C.S. Whittleston, D.J. Wales, Thermodynamics and kinetics of aggregation for the GNNQQNY peptide, J. Am. Chem. Soc. 129 (2007) 16005–16014.
[27] G. Reddy, J.E. Straub, D. Thirumalai, Dynamics of locking of peptides onto growing amyloid fibrils, Proc. Natl. Acad. Sci. U. S. A. 106 (2009) 11948–11953.
[28] A.S. Reddy, M. Chopra, J.J. de Pablo, GNNQQNY-investigation of early steps during amyloid formation, Biophys. J. 98 (2010) 1038–1045.
[29] B. Barz, D.J. Wales, B. Strodel, A kinetic approach to the sequence-aggregation relationship in disease-related protein assembly, J. Phys. Chem. B 118 (2014) 1003–1011.
[30] A. Srivastava, P.V. Balaji, Molecular events during the early stages of aggregation of GNNQQNY: an all atom MD simulation study of randomly dispersed peptides, J. Struct. Biol. 192 (2015) 376–391.
[31] N. Katyal, S. Deep, Inhibition of GNNQQNY prion peptide aggregation by trehalose: a mechanistic view, Phys. Chem. Chem. Phys. 19 (2017) 19120–19138.
[32] J. Lei, R. Qi, L. Xie, W. Xi, G. Wei, Inhibitory effect of hydrophobic fullerenes on the β-sheet-rich oligomers of a hydrophilic GNNQQNY peptide revealed by atomistic simulations, RSC Adv. 7 (2017) 13947–13956.
[33] M. Cecchini, F. Rao, M. Seeber, A. Caflisch, Replica exchange molecular dynamics simulations of amyloid peptide aggregation, J. Chem. Phys. (21) (2004) 10748–10756.
[34] J. Nasica-Labouze, M. Meli, P. Derreumaux, Approach to characterize the early aggregation steps of the amyloid-forming peptide GNNQQNY from the yeast prion Sup-35, PLoS Comput. Biol. 7 (2011) e1002782.
[35] J. Nasica-Labouze, N. Mousseau, Kinetics of amyloid aggregation: a study of the GNNQQNY prion sequence, PLoS Comput. Biol. 8 (2012) e1002782.
[36] K.L. Osborne, M. Bachmann, B. Strodel, Thermodynamic analysis of structural transitions during GNNQQNY aggregation, Proteins 81 (2013) 1141–1155.
[37] J.A. Luiken, P.G. Bolhuis, Primary nucleation kinetics of short fibril-forming amyloidogenic peptides, J. Phys. Chem. B 119 (2015) 12568–12579.
[38] S. Auer, P. 1 Ricchiuto, D. Kashchiev, Two-step nucleation of amyloid fibrils: omnipresent or not? J. Mol. Biol. 422 (2012) 723–730.
[39] D. Petrov, B. Zagrovic, Are current atomistic force fields accurate enough to study proteins in crowded environments? PLoS Comput. Biol. 5 (2014) e1003638.
[40] R.B. Best, W. Zheng, J. Mittal, Balanced proteinâ˜water interactions improve properties of disordered proteins and non-specific protein association, J. Chem. Theory Comput. 10 (2014) 5113–5124.
[41] M. Carballo-Pacheco, A.E. Ismail, B. Strodel, On the applicability of force fields to study the aggregation of amyloidogenic peptides using molecular dynamics simulations, J. Chem. Theory Comput. 14 (2018) 6063–6075.
[42] M. Javanainen, H. Martinez-Seara, I. Vattulainen, Excessive aggregation of membrane proteins in the Martini model, PLoS One 12 (2017) e0187936.
[43] D. Van der Spoel, E. Lindahl, B. Hess, G. Groenhof, A.E. Mark, H.J.C. Berendsen, GROMACS: fast, flexible, and free, J. Comput. Chem. (16) (2005) 1701–1718.
[44] L. Monticelli, S.K. Kandasamy, X. Periole, R.G. Larson, D.P. Tieleman, S.J. Marrink, The MARTINI coarse-grained force field: extension to proteins, J. Chem. Theory Comput. 4 (2008) 819–834.

[45] D.H. de Jong, G. Singh, W.D. Bennett, C. Arnarez, T.A. Wassenaar, L.V. Schafer, X. Periole, D.P. Tieleman, S.J. Marrink, Improved parameters for the MARTINI coarse-grained protein force-field, J. Chem. Theory Comput. 9 (2013) 687–697.
[46] C. Guo, Y. Luo, R. Zhou, G. Wei, Probing the self-assembly mechanism of diphenylalanine-based peptide nanovesicles and nanotubes, ACS Nano 6 (2012) 3907–3918.
[47] M. Seo, S. Rausher, R. Pomes, D. Tieleman, Improving internal peptide dynamics in the coarse-grained MARTINI model: toward large-scale simulations of amyloid- and elastin-like peptides, J. Chem. Theory Comput. 8 (2012) 1774–1785.
[48] C. Guo, Y. Luo, R.H. Zhou, G.H. Wei, Triphenylalanine peptides self-assemble into nanospheres and nanorods that are different from the nanovesicles and nanotubes formed by diphenylalanine peptides, Nanoscale 6 (2014) 2800–2811.
[49] N. Thota, Y.J. Ma, J.W. Jiang, Molecular insights into the self-assembly of short amphiphilic peptides F_mD_n and F_mK_n, RSC Adv. 4 (2014) 60741–60748.
[50] S. Emamyari, F. Kargar, V. Sheikh-hasani, S. Emadi, H. Fazli, Mechanisms of the self-assembly of EAK16-family peptides into fibrillar and globular structures: molecular dynamics simulations from nano- to micro-seconds, Eur. Biophys. J. 44 (2015) 263–276.
[51] Y. Sun, Z. Qian, C. Guo, G. Wei, Amphiphilic peptides A_6K and V_6K display distinct oligomeric structures and self-assembly dynamics: a combined all-atom and coarse-grained simulation study, Biomacromolecules 16 (2015) 2940–2949.
[52] A. Mansbach, A.L. Ferguson, Coarse-grained molecular simulation of the hierarchical self-assembly of π-conjugated optoelectronic peptides, J. Phys. Chem. B 121 (2017) 1684–1706.
[53] A. Jain, C. Globish, S. Verma, C. Peter, Coarse-grained simulations of peptide nanoparticle formation: role of local structure and nonbonded interactions, J. Chem. Theory Comput. 15 (2019) 1453–1462.
[54] S.J. Marrink, H.J. Risselada, S. Yefimov, D.P. Tieleman, A.H. de Vries, The MARTINI force field: coarse grained model for biomolecular simulations, J. Phys. Chem. B 111 (2007) 7812–7824.
[55] W. Humphrey, A. Dalke, K. Schulten, VMD – visual molecular dynamics, J. Mol. Graph. 14 (1996) 33–38.
[56] J. Zierenberg, W. Janke, From amorphous aggregates to polymer bundles: the role of stiffness on structural phases in polymer aggregation, Eur. Phys. Lett. 109 (2015) 28002.
[57] S.J. Marrink, A.H. de Vries, A.E. Mark, Coarse grained model for semiquantitative lipid simulations, J. Phys. Chem. B 108 (2004) 750–760.
[58] S.I.A. Cohen, M. Vendruscolo, C. Dobson, T.P.J. Knowles, From macroscopic measurements to microscopic mechanism of protein aggregation, J. Mol. Biol. 421 (2012) 160–171.
[59] G. Singh, I. Brovchenko, A. Oleinikova, R. Winter, Peptide aggregation in finite systems, Biophys. J. 95 (2008) 3208–3221.
[60] A. Pawar, G. Favrin, Finite size effects in simulations of protein aggregation, PLoS One 3 (2008) e2641.